

## Heterogeneous crystallization of hard and soft spheres near flat and curved walls

K. Sandomirski<sup>1</sup>, S. Walta<sup>1,2</sup>, J. Dubbert<sup>2</sup>, E. Allahyarov<sup>3,4</sup>, A.B. Schofield<sup>5</sup>,  
H. Löwen<sup>3</sup>, W. Richtering<sup>2</sup>, and S.U. Egelhaaf<sup>1,a</sup>

<sup>1</sup> Condensed Matter Physics Laboratory, Heinrich Heine University, 40225 Düsseldorf,  
Germany

<sup>2</sup> Institute of Physical Chemistry, RWTH Aachen University, 52056 Aachen, Germany

<sup>3</sup> Institute for Theoretical Physics II: Soft Matter, Heinrich Heine University,  
40225 Düsseldorf, Germany

<sup>4</sup> Joint Institute for High Temperatures, Russian Academy of Sciences (IVTAN), Moscow  
125412, Russia

<sup>5</sup> School of Physics & Astronomy, The University of Edinburgh, Edinburgh EH9 3JZ, UK

Received 13 December 2013 / Received in final form 10 January 2014

Published online 28 February 2014

**Abstract.** Crystallization represents a long-standing problem in statistical physics and is of great relevance for many practical and industrial applications. It often occurs in the presence of container walls or impurities, which are usually unavoidable or might even be desirable to facilitate crystallization by exploiting heterogeneous nucleation. Heterogeneous nucleation relies on a seed. Here we discuss the role of the seed and concentrate on a very generic situation, namely crystallization of hard and soft colloidal spheres in the presence of flat or curved hard walls. Curvature serves as a simple means to introduce a tunable mismatch between the seed-induced crystal lattice and the thermodynamically-favoured lattice. The mismatch induces distortions and elastic stress, which accumulate while the crystallite grows. This has an important consequence: once the crystallite reaches a critical size, it detaches from the seed allowing it to relax. The relaxed crystal continues to grow in the bulk, but crystallization ceases before reaching the seed, which now represents an impurity. Therefore, while seeds favour nucleation, any mismatch, like the seed curvature or an incommensurate structure, induces unfavourable distortions and can lead to the detachment of the crystallite. An additional mechanism to relax distortions is available to soft spheres, which can exploit their interaction potential and possibly deform. The different multi-step processes have been investigated by confocal microscopy, which provides particle-level information, and compared to computer simulations and theoretical results.

<sup>a</sup> e-mail: [Stefan.Egelhaaf@uni-duesseldorf.de](mailto:Stefan.Egelhaaf@uni-duesseldorf.de)

## 1 Introduction

Understanding disorder-order transitions is not only important from a fundamental point of view, but also relevant for industrial applications. Of special current interest are the kinetics and pathways of such processes with crystallization representing a prominent example. The applications range from material science, namely metallurgy [1–7] and the fabrication of nanoparticles and optical band-gap crystals [8,9], to meteorology [10], medicine, where crystallization can play a central role in pathological and normal conditions [11,12], and biotechnology, where the crystallization of proteins is an important issue [12–26].

Homogeneous crystallization has been investigated experimentally [27–45], by computer simulations [46–61] and has been theoretically described based on classical nucleation theory [62,63] as well as other models [64–67]. For example, the structure of critical nuclei has been studied experimentally [34,36,37] and by computer simulations [51–54]. Furthermore, the nucleation rates have been determined experimentally [36–45] and predicted theoretically [45–51] without full agreement being achieved. Often homogeneous crystallization is dominated by heterogeneous crystallization, since container walls and impurities are almost omnipresent, especially in practical and industrial situations. Heterogeneous crystallization hence is often inevitable or even desirable, which renders it particularly relevant. Heterogeneous nucleation can be induced by flat or curved walls, including individual seed particles [10,68–92], particle assemblies [93–95] or structured walls [9,26,96–104]. The seeds reduce the free energy barrier to nucleation and thus enhance crystallization. However, surfaces and particles can also act as impurities and suppress crystallization [105–110]. This ambiguity between crystallization enhancing and crystallization suppressing properties renders the optimization of processes very complex.

Despite its relevance, quantitative particle-level mechanistic information on heterogeneous crystallization is still sparse. Mainly bulk methods have been applied to investigate crystallization [30–33,38–45,87]. However, to improve the understanding of the underlying processes, microscopic information on the particle level is desired. This can be obtained using colloidal suspensions, which have proven to be powerful model systems [6,7,111–113]. They do not only allow one to tune the particle interactions, but their size range includes the wavelength of visible light and hence they are “visible”. Furthermore, due to their relatively large size, colloidal processes and the particle dynamics are slow enough to be followed in experiments. To travel its own diameter  $\sigma$ , a colloidal particle requires the Brownian time  $\tau_B = \sigma^2/D_0$  (with the diffusion coefficient  $D_0$  in the dilute limit), which is of the order  $\tau_B \sim 10\text{ s}$ . The relatively large size also enables the investigation of heterogeneous crystallization in the presence of surfaces which are smooth on the scale of the crystallizing colloidal particle, while no surface is perfectly flat on an atomic scale. Colloidal crystallization has been investigated in reciprocal space by light scattering [38–45] and in real space by confocal microscopy [35–37,88,89,96,105–108]. Based on sequences of images, the particle locations and trajectories can be determined [114,115] and the structural, dynamic and thermodynamic parameters derived [116,117]. This includes local order parameters, based on which fluid and crystalline particles can be distinguished [49,118,119]. Using confocal microscopy, crystallization can hence be followed on an individual particle level and the results quantitatively compared to simulations and theoretical predictions.

Here we focus on the most basic realization of heterogeneous crystallization: the crystallization of hard and soft spheres in the presence of an unstructured hard wall, which might be flat or curved. In the experiments, hard spheres are realized by a well characterized and frequently-studied model system: sterically-stabilized and fluorescently-labelled polymethylmethacrylate (PMMA) particles (here of diameter

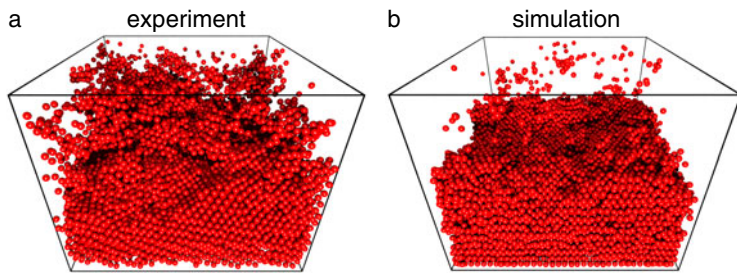


**Fig. 1.** Representation of a hard sphere crystal growing next to a flat hard wall based on (a) confocal microscopy and (b) simulations. Time  $t = 62\tau_B$ , volume fraction  $\phi = 0.52$ . Only crystalline particles are shown and the simulation box is reduced in  $z$  direction.

$\sigma = 1.83 \mu\text{m}$ , hence  $D_0 = 1.03 \times 10^{-9} \text{ cm}^2/\text{s}$  and  $\tau_B = 33 \text{ s}$ , and polydispersity below 4%) suspended in a mixture of cis-decalin and cycloheptyl bromide, whose density and refractive index (almost) match the ones of the particles, with tetrabutylammonium chloride added to screen residual charges [111, 120, 121]. The crystallization of colloidal hard spheres is entropy driven and controlled by only one parameter, the volume fraction  $\phi$  occupied by particles [122]. Hard spheres start to freeze at  $\phi_f = 0.494$  and melt at  $\phi_m = 0.545$  [30, 111]. Microgel particles based on poly(N-isopropylacrylamide) (PNIPAM) serve as soft compressible spheres [123–125]. Their phase behaviour [126–133] is richer than the ones of hard and charged spheres [27, 30, 41, 111], which they contain as limiting cases. Planar container walls, added glass spheres and cylinders are used to study the effect of flat and curved seed surfaces. In the case of spheres and cylinders, the walls of the sample cell are coated with an inhomogeneous film of polydisperse PMMA particles to avoid (faster) heterogeneous nucleation next to the flat wall, while the walls are left untreated to study heterogeneous nucleation in the presence of a flat wall. The hard spheres are imaged and stored in small vials with their bottoms replaced by cover slips [115], which allow for easier homogenization of the samples using a magnetic bar. Despite thorough mixing, up to five partially ordered layers remain on the flat wall or curved seed surface, which is attributed to the favourable wetting of hard walls by hard spheres [41, 71–73]. The soft spheres were kept in temperature-controlled cells [134]. The adsorption of microgels to interfaces [135], in this case a glass surface, has to be take into account.

This mini review is organized as follows: In chapter 2 we discuss heterogeneous crystallization in the presence of a flat smooth wall, which favours crystallization without introducing a mismatch between the thermodynamically-favoured and seed-induced crystallite. Then, heterogeneous crystallization is investigated in situations where strain and elastic stress is accumulated in the growing crystallite due to the curvature of the seed, first curvature in one direction, namely cylindrical seeds (Chap. 3), then curvature in two directions, namely spherical seeds (Chap. 4), are discussed. Particular attention is given to the release of strain by detachment (Chap. 4.2), but also the possibility to release or avoid strain by allowing for softness of the particles (Chap. 5). The findings are briefly summarized in the concluding chapter (Chap. 6).

## 2 Crystallization next to a flat wall

Possibly the most basic realizations of heterogeneous crystallization is hard spheres crystallizing in the presence of a flat and unstructured hard wall (Fig. 1) [68, 71, 87, 88]. In this situation, crystallization starts with a very short induction period. Nucleation is very fast since, in the presence of a wall, no appreciable nucleation

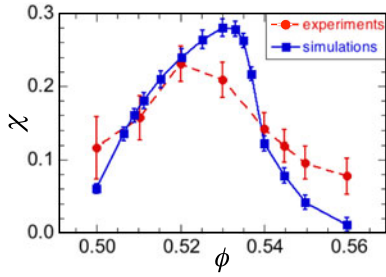


**Fig. 2.** Crystal growth rate  $\chi$  as a function of bulk volume fraction  $\phi$ . The rates have been determined by confocal microscopy (●) and simulations (■). The lines are guides to the eye.

barrier exists [41, 71–74, 136–139]. Subsequently, the crystallite grows with, close to the flat wall as well as throughout the crystal, the (111) crystal plane oriented parallel to the wall. Mainly fcc, but also hcp stacking is observed, which indicates random stacking. Furthermore, only a few defects or grain boundaries exist. On the other hand, homogeneous crystallization in the bulk is negligible; only very few crystalline particles and small clusters occur in bulk, but neither reach the size of a critical nucleus nor significantly affect the propagation of the crystallization front. Hence, in this situation heterogeneous crystallization dominates.

## 2.1 Growth of the crystal and development of a depletion zone

Since nucleation near a hard wall is fast and the subsequent crystal growth relatively slow, the time scales of the two processes are well separated. In this case, thus the observation of crystal growth is hardly affected by other processes, namely heterogeneous nucleation and initial rearrangements. In addition, the effectively one-dimensional geometry renders the situation very simple. Therefore, this scenario allows one to quantitatively investigate crystal growth on an individual-particle level without complications arising from other effects, such as complex interactions, seed curvature, geometry or competing processes.

Exploiting the effectively one-dimensional geometry, the crystal growth rate was determined based on the time evolution of the effective number of crystalline layers  $N_c(t)/N_1$ , where  $N_c(t)$  is the total number of crystalline particles and  $N_1$  the mean number of crystalline particles in a single layer. After a brief induction stage, for an extended period of time  $N_c(t)/N_1$  increases linearly [88]. In the extended linear regime, a growth rate can be extracted;  $\chi = d(N_c(t)/N_1)/d(t/\tau_B)$ . The growth rate  $\chi(\phi)$  displays a non-monotonic behaviour as a function of the volume fraction  $\phi$  with a maximum at  $\phi \approx 0.53$  (Fig. 2). This is consistent with studies on homogeneous crystallization [36, 37, 40–51, 64, 65]. The maximum results from the balance of an increasing thermodynamic driving force [31, 46, 47, 56] and a decreasing mobility [42, 111]. The mobility or, equivalently, the diffusion coefficient  $D(\phi)$  decreases with increasing  $\phi$  due to progressive caging by the particle's neighbours. Caging determines the behaviour of  $\chi(\phi)$  at large  $\phi$  while the increasing thermodynamic driving force dominates at smaller  $\phi$ .

A detailed insight into crystal growth can be obtained considering further parameters. The local volume fraction  $\varphi(z)$ , which here considers the particle volumes located in the particles' centres, allows one to distinguish crystalline and fluid regions (Fig. 3b). At some distance from the wall,  $\varphi(z)$  is essentially constant without pronounced fluctuations, consistent with a disordered fluid with an insignificant fraction of crystalline particles (Figs. 1, 3a). In contrast, in the proximity of the wall,

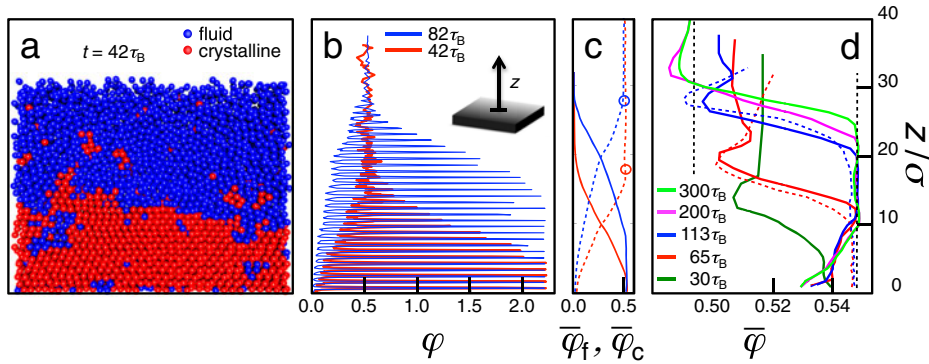


**Fig. 3.** (a) Representation of a cut through the growing crystal with crystalline particles shown in red and fluid particles in blue. The flat wall is located at  $z/\sigma = 0$  and the  $z$ -axis, which is identical for all parts of this figure, is shown on the right. (b) Local volume fraction profile of all particles,  $\varphi(z, t)$ , (c) locally-averaged volume fraction profile of fluid,  $\bar{\varphi}_f(z, t)$  (dashed lines), and of crystalline particles,  $\bar{\varphi}_c(z, t)$  (solid lines), at the same times as in (b), and (d) locally-averaged volume fraction profile of all particles,  $\bar{\varphi}(z, t)$ . The circles in (c) indicate the locations of the depletion zones. The vertical dotted lines in (d) represent the freezing and melting volume fractions. Times  $t$  are as indicated. The volume fraction  $\phi = 0.52$ . All data are obtained by confocal microscopy, except the solid lines in (d) which are obtained by simulations.

pronounced maxima and minima of  $\varphi(z)$  reflect the ordered structure of the crystalline region. The spacing between individual oscillations increases from the crystal-fluid interface ( $\Delta z = 0.902\sigma$ ) toward the wall ( $\Delta z = 0.921\sigma$ ), which corresponds to the temporal evolution of the lattice spacing. This slight expansion of the crystal lattice has also been observed in scattering experiments and model calculations [41–45]. The maxima and minima in  $\varphi(z)$  decay over a range of about 8 to 16 layers. This width of the crystal-fluid interface is consistent with theoretical, simulation and experimental studies [35, 58, 66, 139–142]. As time progresses, the oscillations and hence the crystal-fluid interface are seen to advance into the fluid region. The propagation of the crystal-fluid interface is taken to be represented by the advancing envelope of  $\varphi(z)$ , from which the crystallization rate  $\chi$  can be determined and is found to agree with  $\chi$  determined based on  $N_c(t)/N_1$  (Fig. 2) [88].

Since the spacing and also the width of the maxima and minima of  $\varphi(z)$  change, the locally-averaged volume fraction  $\bar{\varphi}(z)$  provides a more robust way to quantify the progression of the crystal-fluid interface. It is obtained by averaging  $\varphi(z)$  over one period of the oscillations corresponding to one layer of the crystalline phase. The locally-averaged volume fraction of crystalline,  $\bar{\varphi}_c(z)$ , and fluid,  $\bar{\varphi}_f(z)$ , particles can be considered separately (Fig. 3c) and the location of the crystal-fluid interface,  $z_i$ , identified with the position where  $\bar{\varphi}_c(z_i) = \bar{\varphi}_f(z_i)$ . Based on the progression of  $z_i(t)$  the growth rate  $\chi$  can be determined, which also agrees with the growth rates  $\chi$  determined as described above (Fig. 2) [88].

A close inspection of the locally-averaged volume fraction  $\bar{\varphi}(z)$  (Fig. 3c, circles) shows a dip of about 0.01 in the fluid next to the advancing crystal-fluid interface which extends over about  $5\sigma$  (Fig. 3d, note the different scales of the density axes). This is a direct indication for a depletion zone, which has previously been predicted or induced indirectly only [31, 45, 64]. The depletion zone is located in front of the advancing crystal-fluid interface and persists while the crystal grows but disappears at long times when a stable interface position is reached.

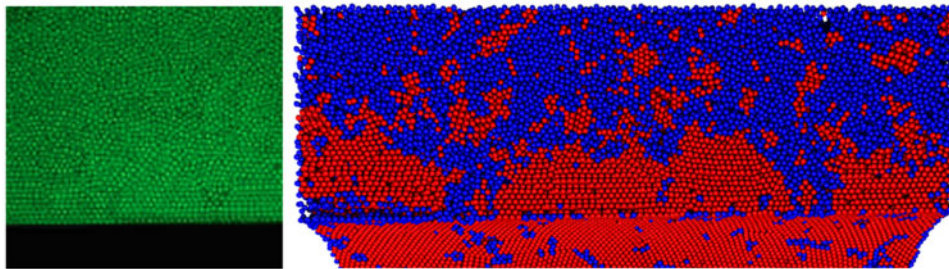


**Fig. 4.** Hard sphere crystal growing on a cylindrical seed (a) as observed in a radial slice by confocal microscopy and (b) corresponding rendered image, which also shows part of the layer covering the cylinder. Crystalline particles are shown in red and fluid particles in blue. Particle diameter  $\sigma = 1.83 \mu\text{m}$ , cylinder diameter  $\sigma_{\text{cyl}} = 42 \sigma$ , time  $t \approx 330 \tau_B$ , volume fraction  $\phi = 0.53$ .

## 2.2 No induced distortions

At the wall as well as throughout the crystal, the (111) plane is oriented parallel to the wall. While this orientation is induced by the wall, it represents the only effect of the wall on the structure of the crystal. The slight relaxation of the crystal lattice while the crystal grows has also been observed in homogeneously nucleated crystals [42–45] and is hence not related to the presence of the wall. Therefore, although crystallization is initiated at the wall, the structure of the crystal is unaffected by the presence of the flat wall and, in particular, the crystal does not contain any distortions caused by the wall.

## 3 Crystallization next to a cylinder

To study the mismatch between the seed-induced and thermodynamically-favoured crystal structures, curvature of the wall is introduced. The wall's curvature can be controlled and adjusted easily and hence allows one to tune the mismatch in a broad range. It introduces an additional parameter, namely the radius of curvature or, equivalently, the seed diameter  $\sigma_{\text{seed}}$ .

First, the effect of curvature in one direction is investigated by adding cylindrical smooth seeds [50, 91]. Crystallization starts on the cylinder surface with the (111) plane parallel to the surface (Fig. 4). The crystal-fluid interface advances into the bulk fluid, while only few crystalline particles and crystalline clusters exist in the fluid phase. Thus, cylindrical seeds can also induce heterogeneous crystallization. However, in the heterogeneously-grown crystals the lattice planes are curved, which is imposed by the curvature of the cylinder surface.

### 3.1 Growth of the crystal

Crystallization in the presence of cylindrical seeds is quantified by the local volume fraction of crystalline particles,  $\varphi_c(r)$ , again considering the whole particle volumes located in the particles' centres (Fig. 5). Close to the cylinder pronounced maxima and minima indicate an ordered crystalline region, while further from the cylinder  $\varphi_c(r)$  decays to almost zero and also the pronounced oscillations disappear, consistent with the presence of a disordered fluid. With time, the oscillations extend further

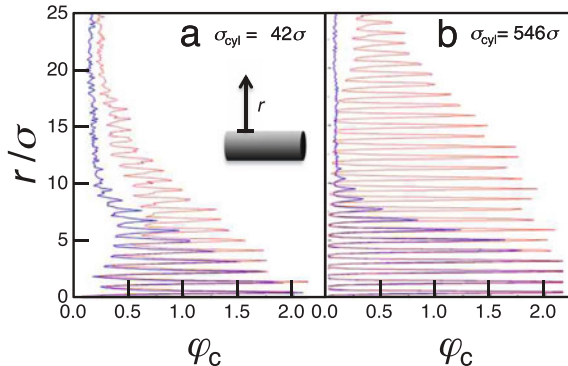


**Fig. 5.** Local volume fraction of crystalline particles,  $\varphi_c(z,t)$ , as a function of the distance from the cylinder surface  $r/\sigma$  at an early time (blue lines) and  $\Delta t \approx 330 \tau_B$  later (red lines) as determined by confocal microscopy. Cylinder diameters are (a)  $\sigma_{cyl} = 42\sigma$  and (b)  $\sigma_{cyl} = 546\sigma$ , volume fraction  $\phi = 0.53$ .

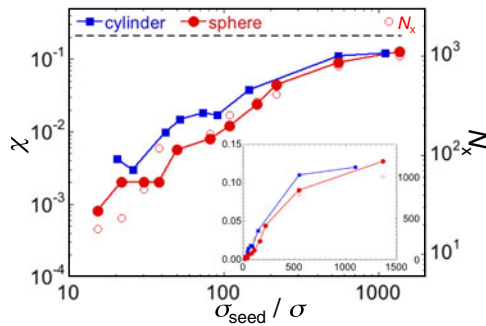


**Fig. 6.** Crystal growth rate  $\chi$  as a function of normalized seed diameter  $\sigma_{seed}/\sigma$  for cylindrical (■) and spherical seeds (●) as observed by confocal microscopy. The horizontal dashed line indicates the experimentally determined growth rate  $\chi$  in the presence of a flat wall (Fig. 2). Also shown is the average patch size, in terms of the number of particles per patch  $N_x$ , which are observed in the second layer surrounding the spherical seed (○). Volume fraction  $\phi = 0.53$ . Lines are guides to the eye. The inset shows the same data in a lin-lin plot.

into the sample, indicating the growth of the crystal. The number of maxima of  $\varphi_c(r)$  increases linearly with time  $t$  for an extended period [91]. The slope of the linear time dependence of  $\varphi_c(r)$  corresponds to the crystal growth rate  $\chi$ . (Similar values of  $\chi$  are obtained by considering the increase of the number of crystalline particles [91].)

For larger cylinders, the crystalline region extends further into the fluid and also proceeds faster into the fluid (Fig. 5). The growth rate  $\chi$  increases with the diameter of the cylinder,  $\sigma_{cyl}$  (Fig. 6) [79, 91]. For very small cylinders with a size comparable to the size of the particles, the case of homogeneous crystallization in the presence of impurities is approached [79, 105–110]. As the diameter of the cylinder increases and thus the curvature of the seed surface decreases, the crystallization rate first shows a modest increase followed by a more pronounced increase around  $\sigma_{cyl} \approx 200\sigma$ . Subsequently,  $\chi$  saturates, slowly approaching the rate observed in the presence of a flat wall.

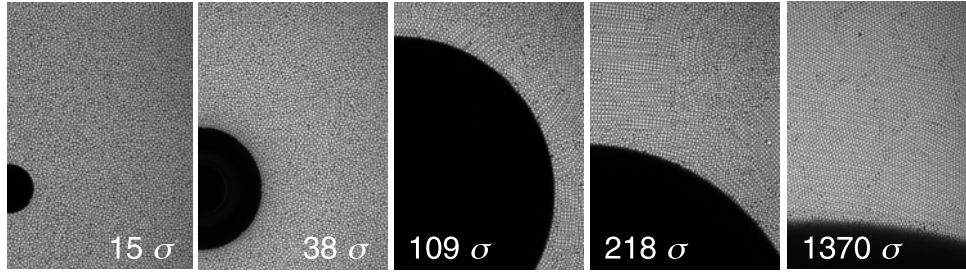


**Fig. 7.** Hard sphere crystals growing on spherical seeds of different diameters  $\sigma_{\text{sph}}$  (as indicated). Particle diameter  $\sigma = 1.83 \mu\text{m}$ , time  $t = 545 \tau_B$ , volume fraction  $\phi = 0.53$ .

### 3.2 Induced distortions

Compared to homogeneous crystallization, cylinders with  $\sigma_{\text{cyl}} \gtrsim 30 \sigma$  enhance crystallization. Although they favour crystallization, the curvature of the cylinder surface leads to curved crystal planes and hence induces considerable distortions in the growing crystallite. The distortions have important consequences on the crystallization process, which will be discussed below (Sect. 4.2).

## 4 Crystallization next to a sphere

Heterogeneous crystallization in the presence of a sphere, i.e. a surface isotropically curved in two directions, has been studied analytically in the framework of classical nucleation theory (e.g. [69]) and using simulations [79]. Furthermore, confocal microscopy has been used to study small spherical impurities, which hinder crystallization [105–108], or impurities which are swept to the grain boundaries [143]. Very small spheres with a size comparable to the colloidal particles are expected to have a similar effect as polydispersity and thus reduce the crystallization rate [38, 39, 44, 46, 109, 110]. Slightly larger spheres, but still with a significant surface curvature, also hinder crystallization and act as impurities [105–108]. In contrast, large spheres favour crystallization. The growth rate is expected to increase with increasing size, that is decreasing surface curvature, approaching the limit of a flat wall [79, 80, 89, 90].

A qualitative inspection of confocal microscopy images (Figs. 7, 8) reveals a significant effect of the seed curvature on heterogeneous crystallization [80]. The size of the crystallites increases with increasing seed size or, equivalently, decreasing surface curvature. In the presence of very small spheres ( $\sigma_{\text{sph}} \lesssim 20 \sigma$ ), only a few small crystallites or ordered layers cover the seeds. The fraction of crystal-like particles in the vicinity of very small seeds is smaller than far away from the seeds. Hence these seeds actually prevent crystallization and thus act as impurities. Upon increasing the seed size ( $\sigma_{\text{sph}} \gtrsim 150 \sigma$ ), heterogeneous crystallization is observed with extended crystal growth occurring for  $\sigma_{\text{sph}} \gtrsim 300 \sigma$ . Thus, crystallization is only favoured by large seeds, which have a size much larger than the colloidal particles, rather in the expected range of a critical nucleus.

### 4.1 Growth of the crystal

Crystal growth is again quantified by the evolution of  $\varphi_c(r, t)$  (Fig. 9). For small spherical seeds, a small number of oscillations in  $\varphi_c(r, t)$  indicates only a few crystallites

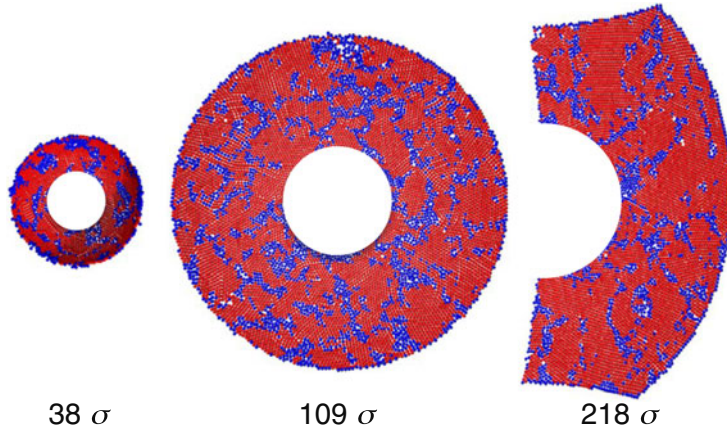


**Fig. 8.** Second layer surrounding spherical seeds of different diameters  $\sigma_{\text{sph}}$  (as indicated) projected onto a plane. Rendered images with crystalline particles shown in red and fluid particles in blue. Time  $t = 545 \tau_B$ , volume fraction  $\phi = 0.53$ .

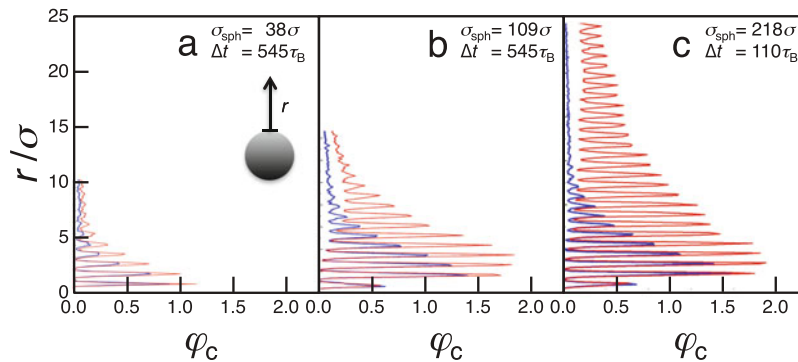


**Fig. 9.** Local volume fraction of crystalline particles,  $\varphi_c(r, t)$  as a function of the distance from the sphere surface  $r/\sigma$  at an early time (blue lines) and  $\Delta t = 545 \tau_B$  ( $\sigma_{\text{sph}} = 38, 109 \sigma$ ),  $\Delta t = 110 \tau_B$  ( $\sigma_{\text{sph}} = 218 \sigma$ ) (red lines) as determined by confocal microscopy. Sphere diameters are (a)  $\sigma_{\text{sph}} = 38 \sigma$ , (b)  $\sigma_{\text{sph}} = 109 \sigma$  and (c)  $\sigma_{\text{sph}} = 218 \sigma$ , volume fraction  $\phi = 0.53$ .

and very few ordered layers covering the highly curved seed. Furthermore, with time the oscillations and hence the crystallites do not significantly advance into the fluid. Only larger seeds with  $\sigma_{\text{sph}} \gtrsim 150 \sigma$  induce appreciable heterogeneous crystallization with oscillations in  $\varphi_c(r, t)$  implying that crystalline layers significantly extend into the fluid. Although the crystalline layers progress into the fluid, crystal growth is very slow, with only a modest progression of the fluid-crystal interface. Only for diameters  $\sigma_{\text{sph}} \gtrsim 300 \sigma$ , the seeds induce considerable crystallization with a significantly advancing front.

Based on the increasing number of oscillations, corresponding to an increasing number of crystalline layers, the growth rate  $\chi$  with which the front of the crystal moves into the fluid phase can be determined (Fig. 6, red filled circles). Similar values for  $\chi(\sigma_{\text{sph}})$  are obtained based on the progression of the envelope of  $\varphi_c(r, t)$  or the evolution of the number of crystalline layers [80]. Upon increasing the seed diameter  $\sigma_{\text{sph}}$ , the rate  $\chi(\sigma_{\text{sph}})$  shows a modest increase, followed by a more significant increase for  $100 \sigma \lesssim \sigma_{\text{sph}} \lesssim 1000 \sigma$  with a subsequent saturation toward the rate observed in

the presence of a flat wall,  $\chi(\sigma_{\text{sph}} \rightarrow \infty) \approx 0.21$ . The increase occurs at larger seed sizes than observed in simulations [79]. This might be due to polydispersity or the different number of defects initially present. A comparison with the results for a cylindrical seed (Fig. 6), for this criterion to determine  $\chi$ , reveals about two times lower rates than for cylindrical seeds of the same small diameter  $\sigma_{\text{seed}}$  while for larger  $\sigma_{\text{seed}}$  the rates approach each other. This is attributed to two versus only one principal curvature direction. Furthermore, it is consistent with previous simulation results which showed enhanced crystallization in the presence of cylindrical seeds compared to spherical seeds [79].

The seed curvature has also a strong effect on the number and size of the individual crystallites (Fig. 7). This is illustrated by the crystal-like or liquid-like properties of the particles in the second layer (Fig. 8). The crystalline layers exhibit a hexagonal structure with the (111) plane bending around the curved seed surface. The curvature results in small crystallites with many grain boundaries and defects. Individual crystallites are identified by the orientation of their crystal lattice. The crystallites' average cross-sectional area in the second layer, quantified by the number of particles per patch  $N_x(\sigma_{\text{sph}})$ , was determined. The average patch size, i.e.  $N_x(\sigma_{\text{sph}})$ , increases with increasing seed diameter (Fig. 6, red open circles). Thus, nearly flat seeds produce larger crystals than highly curved seeds. Furthermore, the curvature of the seed determines the number of crystallites. The dependence of  $N_x(\sigma_{\text{sph}})$  on seed diameter is very similar to the dependence of the crystal growth rate  $\chi(\sigma_{\text{sph}})$  with a modest initial increase followed by a more pronounced increase. Thus not only the growth rate depends on the seed diameter, but also the size and number of crystallites.

#### 4.2 Induced distortions

A curved seed can enhance crystallization, but also induces distortions in the crystal lattice. The latter can lead to the detachment of the nucleus from the seed before the nucleus reaches its critical size [79]. This has important consequences: First, the nucleus must reach its critical size in bulk and thus under conditions of homogeneous crystallization. Second, the seed can initiate another nucleus and thus act as a “crystallization catalyst”.

To investigate these issues in more detail, crystallization was followed for a much longer time, almost to its completion [81]. Confocal microscopy and Brownian dynamics simulations consistently indicate that, in the presence of added large spheres, crystallization proceeds in several stages. First, heterogeneous crystallization is initiated at the seed surface, as described in detail above. The seed-induced crystal structure with its curved crystal planes does, however, not match the thermodynamically-favoured crystal structure. The mismatch induces distortions and thus elastic stress, which accumulates while the crystallite grows. Once the elastic energy penalty reaches the interfacial energy gained by growing on the seed, the crystallite releases the elastic stress by detaching from the seed. The heterogeneous growth of the crystallite is thus limited to a maximum size. The observed detachment size is given by the balance between elastic and interfacial energies [81]. The detached and relaxed crystallite continues to grow in the bulk. As a consequence, the melted region between the seed and the detached crystallite starts to refreeze. However, crystallization ceases before reaching the added large sphere, which prevents complete crystallization and hence now acts as an impurity. This indicates an intricate balance between heterogeneous and homogeneous crystallization with the added large particle acting initially as crystallization-enhancing seed and, later, as crystallization-impeding impurity. Both phenomena are observed in the same multi-step process with the particle changing its

role when the crystallite detaches from the seed, which hence represents the crucial turning point in this multi-stage process.

The detachment is initiated by a mismatch between the seed-induced and thermodynamically-favoured crystal structure. The mismatch might be due to seed curvature or, e.g., incommensurate unit cell structures or sizes. A crystal lattice mismatch is very common, hard to avoid, especially if the equilibrium crystal structure is unknown, or even desired for material property reasons. Therefore, this multi-step scenario is of great technological relevance, in particular as it is expected to be essentially independent of what causes the mismatch and hence the findings are applicable to many situations of heterogeneous crystallization. For the rational design and production of materials it is furthermore interesting that the crystallite size can be controlled through the seed size.

Since the crystallite detaches from the seed, the seed might repeatedly initiate heterogeneous nucleation and hence act as “crystallization catalyst” [79]. In the present case, however, the detached crystallite grows toward its seed and thus prevents it from again acting as seed. This could be avoided by removing the crystallite using, e.g., gravity or mechanical forces, such as shear. While this is difficult in a concentrated suspension, it might be possible in a dilute fluid. This requires a large coexistence region, which occurs for example in colloid-polymer mixtures [144].

## 5 Soft spheres

As discussed, a curved seed introduces strain in the crystal lattice of the heterogeneously growing crystallite, which can be released after the crystallite detaches from the seed [79–81,145]. Another mechanism to release or avoid strain is offered by softness, through the particle-particle interaction potential or the deformability of the particles [92]. This effect can be investigated by following the crystallization of soft spheres instead of hard spheres. Microgel particles represent tunable soft spheres [123–125], which can be sensitive to variations in temperature, pH, ionic strength or hydrostatic pressure [146,147]. They thus display important differences to hard spheres. They are swollen by the solvent and the segment density decays smoothly toward their surface, which leads to compressible spheres with a fuzzy, i.e. soft, interface. The cross-link densities of their core and shell determine the size and softness, ranging from hard spheres (thin shell, large cross-link density) to very soft particles (thick shell, low cross-link density). They might also be charged, which significantly extends the range of the softness [125–130]. Due to the additional parameters, such as the strength and range of the electrostatic interactions or the softness, their phase behaviour becomes richer [126–132], but still includes the hard sphere limit. Furthermore, the delicate dependence of the phase behaviour on these parameters implies that the details of the particle synthesis are important and small differences in the synthesis can result in significant changes in the phase behaviour.

Here, we discuss the heterogeneous crystallization of microgels based on poly(N-isopropylacrylamide) (PNIPAM) and cross-linked by N,N'-methylene bis(acrylamide) (up to 6 mol%). They are fluorescently labelled via copolymerization of NIPAM with methacryloyloxyethylthiocarbomylrhodamine B and have an almost homogeneous segment density resulting in a fuzzy surface that however, is very narrow (about 36 nm) compared to the particles hydrodynamic radius ( $\sigma/2 = 287$  nm, implying  $\tau_B \approx 0.43$  s, with a polydispersity of about 9%, determined by static and dynamic light scattering) and thus sharper than for common PNIPAM microgels although not as steep as for homogeneous hard spheres. These microgels can hence serve as a model system for compressible spheres with a rather sharply-defined surface.

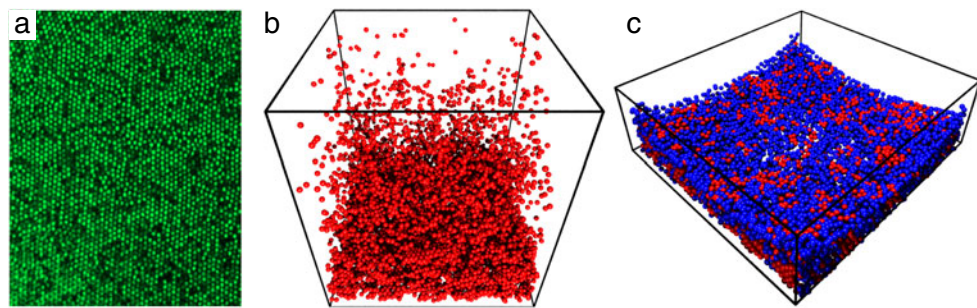


**Fig. 10.** Soft sphere crystals growing in the presence of a flat or curved wall as observed by confocal microscopy. (a) Slice in the vicinity of and parallel to a flat wall and (b) rendered image with the flat wall located at the bottom of the box and only crystalline particles shown. (c) Rendered image showing crystalline (red) and fluid (blue) particles in the vicinity of a spherical seed of diameter  $\sigma_{\text{sph}} = 157 \sigma$ . Particle diameter  $\sigma = 0.574 \mu\text{m}$ , weight fraction  $\phi_w = 3.99 \text{ wt\%}$ .

Crystals formed by soft spheres have been studied by confocal microscopy [92, 130, 131]. In the presence of a flat wall, heterogeneous crystallization in the vicinity of the wall dominates over homogeneous crystallization in the bulk (Fig. 10a,b) [92]. The behaviour resembles the crystallization of hard spheres (Sect. 2). However, a larger number of crystallites and thus of grain boundaries and defects exist, which is attributed to the softness of the particles. Preliminary experiments show that spherical seeds initiate heterogeneous crystallization (Fig. 10c) [92]. A detailed investigation of crystallization of soft spheres in the presence of spherical seeds is ongoing.

## 6 Conclusions

In heterogeneous crystallization a central role is played by the seed. A very generic realization of a seed is represented by smooth flat or curved walls. Crystallization is favoured by flat and curved walls, with the growth rate increasing with decreasing curvature. While flat walls do not induce strain in the growing crystallites, curved walls lead to distortions and accumulating elastic stress as the crystallites grow. Once the elastic stress reaches the energy gained by growing on the (curved) surface, the crystallite detaches from the seed. The detached and relaxed crystallite subsequently continues to grow in bulk. While this multi-step scenario was discussed for smooth flat and curved walls, it is expected to occur in any situation where the seed induces a mismatch compared to the thermodynamically-favoured crystal lattice. In practice, a perfect match is very difficult to achieve and, furthermore, the thermodynamically-favoured crystal structure might even be unknown or not desirable due to material property reasons. The presented scenario can be exploited to control material properties and thus is expected to be of great technological relevance.

We thank K. Binder (Mainz), R.P.A. Dullens (Oxford), J. Horbach (Düsseldorf), M. Oettel (Tübingen) T. Palberg (Mainz), C.P. Royall (Bristol), T. Schilling (Luxembourg), and H.J. Schöpe (Mainz) for helpful discussions and the Centre for Advanced Imaging (University Düsseldorf) for providing time on the confocal microscope. This work was supported by the Deutsche Forschungsgemeinschaft (DFG) within the priority programme SPP 1296. A.B.S. is partially funded by the UK Engineering and Physical Sciences Research Council (grant EP/J007404/1) and E.A. by the US Department of Energy (grant DE-FG02-05ER46244).

## References

1. H. Emmerich, H. Löwen, R. Wittkowski, T. Gruhn, G.I. Tóth, G. Tegze, L. Gránásy, *Adv. Phys.* **61**, 665 (2012)
2. H. Emmerich, K. Binder, B. Nestler, *Phil. Mag. Lett.* **87**, 791 (2007)
3. D.G. McCartney, *Int. Mater. Rev.* **34**, 247 (1989)
4. A.L. Greer, A.M. Bunn, A. Tronche, P.V. Evans, D.J. Bristow, *Acta Mater.* **48**, 2823 (2000)
5. K.F. Kelton, A.L. Greer, D.M. Herlach, D. Holland-Moritz, *MRS Bull.* **29**, 940 (2004)
6. P. Wette, I. Klassen, D. Holland-Moritz, T. Palberg, S.V. Roth, D.M. Herlach, *Phys. Rev. E* **79**, 010501 (2009)
7. D.M. Herlach, I. Klassen, P. Wette, D. Holland-Moritz, *J. Phys.: Condens. Matter* **22**, 153101 (2010)
8. A. van Blaaderen, K.P. Velikov, J.P. Hoogenboom, D.L.J. Vossen, A. Yethiraj, R. Dullens, T. van Dillen, A. Polman, *Photonic Crystals and Light Localization in the 21th Century*, edited by C.M. Soukoulis (Kluwer Academic Publishers, 2001)
9. N.V. Dzhomkina, G.J. Vancso, *Soft Matter* **1**, 265 (2005)
10. U. Dusek, G.P. Frank, L. Hildebrandt, J. Curtius, J. Schneider, S. Walter, D. Chand, F. Drewnick, S. Hings, D. Jung, S. Borrmann, M.O. Andreae, *Science* **312**, 1375 (2006)
11. A. Pande, J. Pande, N. Asherie, A. Lomakin, O. Ogun, J. King, G.B. Benedek, *Proc. Natl. Acad. Sci. (US)* **98**, 6116 (2001)
12. J.P.K. Doye, W.C.K. Poon, *Curr. Opin. Coll. Interface Sci.* **11**, 40 (2006)
13. M.C. Wiener, *Methods* **34**, 364 (2004)
14. E.H. Snell, J.R. Hellwell, *Rep. Prog. Phys.* **68**, 799 (2005)
15. R.P. Sear, *J. Phys.: Condens. Matter* **19**, 033101 (2007)
16. M. Ataka, S. Tanaka, *Biopol.* **25**, 337 (1986)
17. S. Tanaka, M. Yamamoto, K. Kawashima, K. Ito, R. Hayakawa, M. Ataka, *J. Cryst. Growth* **168**, 44 (1996)
18. S. Tanaka, M. Yamamoto, K. Ito, R. Hayakawa, M. Ataka, *Phys. Rev. E* **56**, R67 (1997)
19. S. Tanaka, K. Ito, R. Hayakawa, M. Ataka, *J. Chem. Phys.* **111**, 10330 (1999)
20. S. Tanaka, M. Ataka, *J. Chem. Phys.* **117**, 3504 (2002)
21. S. Tanaka, S.U. Egelhaaf, W.C.K. Poon, *Phys. Rev. Lett.* **92**, 128102 (2004)
22. W.C.K. Poon, S.U. Egelhaaf, P.A. Beales, A. Salonen, L. Lawyer, *J. Phys.: Condens. Matter* **12**, L569 (2000)
23. H. Sedgwick, K. Kroy, A. Salonen, M.B. Robertson, S.U. Egelhaaf, W.C.K. Poon, *Eur. Phys. J. E* **16**, 77 (2005)
24. H. Sedgwick, J.E. Cameron, W.C.K. Poon, S.U. Egelhaaf, *J. Chem. Phys.* **127**, 125102 (2007)
25. C. Goegelein, D. Wagner, F. Cardinaux, G. Nägele, S.U. Egelhaaf, *J. Chem. Phys.* **136**, 015102 (2012)
26. D.S. Tsekova, D.R. Williams, J.Y.Y. Heng, *Chem. Eng. Sci.* **77**, 201 (2012)
27. S. Hachisu, Y. Kobayashi, A. Kose, *J. Coll. Interface Sci.* **42**, 342 (1973)
28. J. Yamanaka, M. Murai, Y. Iwayama, M. Yonese, K. Ito, T. Sawada, *J. Am. Chem. Soc.* **126**, 7156 (2004)
29. P. Schall, I. Cohen, D.A. Weitz, F. Spaepen, *Science* **305**, 1944 (2004)
30. P.N. Pusey, W. van Megen, *Nature* **320**, 340 (1986)
31. S. Derber, T. Palberg, K. Schätzel, J. Vogel, *Physica A* **235**, 204 (1997)
32. Z. Cheng, P.M. Chaikin, J. Zhu, W.B. Russel, W.V. Meyer, *Phys. Rev. Lett.* **88**, 015501 (2002)
33. V.C. Martelozzo, A. Schofield, W.C.K. Poon, P.N. Pusey, *Phys. Rev. E* **66**, 021408 (2002)
34. L. Assoud, F. Ebert, P. Keim, R. Messina, G. Maret, H. Löwen, *Phys. Rev. Lett.* **102**, 238301 (2009)
35. R.P.A. Dullens, D.G.A.L. Aarts, W.K. Kegel, *Phys. Rev. Lett.* **97**, 228301 (2006)
36. U. Gasser, E.R. Weeks, A. Schofield, P.N. Pusey, D.A. Weitz, *Science* **292**, 258 (2001)
37. U. Gasser, *J. Phys.: Condens. Matter* **21**, 203101 (2009)

38. H.J. Schöpe, G. Bryant, W. van Megen, Phys. Rev. E **74**, 060401 (2006)
39. S. Iacopini, T. Palberg, H.J. Schöpe, Phys. Rev. E **79**, 010601 (2009)
40. T. Palberg, Curr. Opin. Coll. Interface Sci. **2**, 607 (1997)
41. T. Palberg, J. Phys.: Condens. Matter **11**, R323 (1999)
42. J.L. Harland, W. van Megen, Phys. Rev. E **55**, 3054 (1997)
43. H.J. Schöpe, G. Bryant, W. van Megen, Phys. Rev. Lett. **96**, 175701 (2006)
44. H.J. Schöpe, G. Bryant, W. van Megen, J. Chem. Phys. **127**, 084505 (2007)
45. B.J. Ackerson, K. Schätzel, Phys. Rev. E **52**, 6448 (1995)
46. S. Auer, D. Frenkel, Nature **409**, 1020 (2001)
47. S. Auer, D. Frenkel, J. Phys.: Condens. Matter **14**, 7667 (2002)
48. S. Auer, W.C.K. Poon, D. Frenkel, Phys. Rev. E **67**, 020401 (2003)
49. S. Auer, D. Frenkel, J. Chem. Phys. **120**, 3015 (2004)
50. S. Auer, D. Frenkel, Ann. Rev. Phys. Chem. **55**, 333 (2004)
51. S. Auer, D. Frenkel, Adv. Polym. Sci. **173**, 149 (2005)
52. P.R. ten Wolde, M.J. Ruiz-Montero, D. Frenkel, Phys. Rev. Lett. **75**, 2714 (1995)
53. P.R. ten Wolde, M.J. Ruiz-Montero, D. Frenkel, J. Chem. Phys. **104**, 9932 (1996)
54. T. Schilling, H.J. Schöpe, M. Oettel, G. Opletal, I. Snook, Phys. Rev. Lett. **105**, 025701 (2010)
55. H. Shintani, H. Tanaka, Nature Phys. **2**, 200 (2006)
56. P.N. Pusey, E. Zaccarelli, C. Valeriani, E. Sanz, W.C.K. Poon, M.E. Cates, Phil. Trans. R. Soc. A **367**, 4993 (2009)
57. E. Zaccarelli, C. Valeriani, E. Sanz, W.C.K. Poon, M.E. Cates, P.N. Pusey, Phys. Rev. Lett. **103**, 135704 (2009)
58. T. Zykova-Timan, J. Horbach, K. Binder, J. Chem. Phys. **133**, 014705 (2010)
59. E. Sanz, C. Valeriani, E. Zaccarelli, W.C.K. Poon, P.N. Pusey, M.E. Cates, Phys. Rev. Lett. **106**, 215701 (2011)
60. C. Valeriani, E. Sanz, E. Zaccarelli, W.C.K. Poon, M.E. Cates, P.N. Pusey, J. Phys.: Condens. Matter **23**, 194117 (2011)
61. T. Schilling, S. Dorosz, H.J. Schöpe, G. Opletal, J. Phys.: Condens. Matter **23**, 194120 (2011)
62. R. Becker, W. Döring, Ann. Physik **24**, 719 (1935)
63. D. Turnbull, J.C. Fisher, J. Chem. Phys. **17**, 71 (1949)
64. N.M. Dixit, C.F. Zukoski, Phys. Rev. E **64**, 041604 (2001)
65. N.M. Dixit, C.F. Zukoski (2002) Phys. Rev. E **66**, 051602
66. A. Härtel, M. Oettel, R.E. Rozas, S.U. Egelhaaf, J. Horbach, H. Löwen, Phys. Rev. Lett. **108**, 226101 (2012)
67. D.W. Oxtoby, *Liquids, Freezing and Glass Transition*, edited by J.P. Hansen, D. Levesque, J. Zinn-Justin, Les Houches 1989 Session LI (North Holland, Amsterdam, 1991)
68. D. Turnbull, J. Chem. Phys. **18**, 198 (1950)
69. N.H. Fletcher, J. Chem. Phys. **29**, 572 (1958)
70. G. Navascués, P. Tarazona, J. Chem. Phys. **75**, 2441 (1981)
71. M. Franke, A. Lederer, H.J. Schöpe, Soft Matter **7**, 11267 (2011)
72. M. Heni, H. Löwen, Phys. Rev. E **60**, 7057 (1999)
73. S. Auer, D. Frenkel, Phys. Rev. Lett. **91**, 015703 (2003)
74. D.J. Courtemanche, F. van Swol, Phys. Rev. Lett. **69**, 2078 (1992)
75. R.P. Sear, Phys. Rev. E **70**, 021605 (2004)
76. R.P. Sear, J. Phys.: Condens. Matter **17**, 3997 (2004)
77. R.P.A. Dullens, W.K. Kegel, Phys. Rev. Lett. **92**, 195702 (2004)
78. R.P.A. Dullens, M.C.D. Mourad, D.G.A.L. Aarts, J.P. Hoogenboom, W.K. Kegel, Phys. Rev. Lett. **96**, 028304 (2006)
79. A. Cacciuto, S. Auer, D. Frenkel, Nature **428**, 404 (2004)
80. K. Sandomirski, E. Allahyarov, H. Löwen, S.U. Egelhaaf (in preparation)
81. E. Allahyarov, K. Sandomirski, S.U. Egelhaaf, H. Löwen (in preparation)
82. D. Winter, P. Virnau, K. Binder, Phys. Rev. Lett. **103**, 225703 (2009)

83. H.J. Schöpe, P. Wette, Phys. Rev. E **83**, 051405 (2011)
84. D. Deb, A. Winkler, M.H. Yamani, M. Oettel, P. Virnau, K. Binder, J. Chem. Phys. **134**, 214706 (2011)
85. A. Engelbrecht, R. Meneses, H.J. Schöpe, Soft Matter **7**, 5685 (2011)
86. T. Palberg, M.R. Maaroufi, A. Stipp, H.J. Schöpe, J. Chem. Phys. **137**, 094906 (2012)
87. P. Wette, A. Engelbrecht, R. Salh, I. Klassen, D. Menke, D.M. Herlach, S.V. Roth, H.J. Schöpe, J. Phys.: Condens. Matter **21**, 464115 (2009)
88. K. Sandomirski, E. Allahyarov, H. Löwen, S. U. Egelhaaf, Soft Matter **7**, 8050 (2011)
89. F. Ziese, G. Maret, U. Gasser, J. Phys.: Condens. Matter **25**, 375105 (2013)
90. A. Engelbrecht, H.J. Schöpe, Soft Matter **8**, 11034 (2012)
91. S. Walta, K. Sandomirski, W. Richtering, S.U. Egelhaaf (in preparation)
92. K. Sandomirski, J. Dubbert, S. Walta, W. Richtering, S.U. Egelhaaf (in preparation)
93. M. Hermes, E.C.M. Vermolen, M.E. Leunissen, D.L.J. Vossen, P.D.J. van Oostrum, M. Dijkstra, A. van Blaaderen, Soft Matter **7**, 4623 (2011)
94. G. Kahl, H. Löwen, J. Phys.: Condens. Matter **21**, 464101 (2009)
95. S. van Teeffelen, C.N. Likos, H. Löwen, Phys. Rev. Lett. **100**, 108302 (2008)
96. J.P. Hoogenboom, A.K. van Langen-Suurling, J. Romijn, A. van Blaaderen, Phys. Rev. E **69**, 051602 (2004)
97. K.H. Lin, J.C. Crocker, V. Prasad, A. Schofield, D.A. Weitz, T.C. Lubensky, A.G. Yodh, Phys. Rev. Lett. **85**, 1770 (2000)
98. M. Heni, H. Löwen, Phys. Rev. Lett. **85**, 3668 (2000)
99. W.S. Xu, Z.Y. Sun, L.J. An, J. Chem. Phys. **132**, 144506 (2010)
100. L. Assoud, R. Messina, H. Löwen, Mol. Phys. **109**, 1385 (2011)
101. G.I. Toth, G. Tegze, T. Pusztai, L. Granasy, Phys. Rev. Lett. **108**, 025502 (2012)
102. A. Cacciuto, D. Frenkel, Phys. Rev. E **72**, 041604 (2005)
103. D. Frenkel, Nature **443**, 641 (2006)
104. S. Dorosz, T. Schilling, J. Chem. Phys. **136**, 044702 (2012)
105. V.W.A. de Villeneuve, R.P.A. Dullens, D.G.A.L. Aarts, E. Groeneveld, J.H. Scherff, W.K. Kegel, H.N.W. Lekkerkerker, Science **309**, 1231 (2005)
106. V.W.A. de Villeneuve, D. Verboekend, R.P.A. Dullens, D.G.A.L. Aarts, W.K. Kegel, H.N.W. Lekkerkerker, J. Phys.: Condens. Matter **17**, S3371 (2005)
107. R.P.A. Dullens, V.W.A. de Villeneuve, M.C.D. Mourad, A.V. Petukhov, W.K. Kegel, Eur. Phys. J. Appl. Phys. **44**, 21 (2008)
108. V.W.A. de Villeneuve, L. Derendorp, D. Verboekend, E.C.M. Vermolen, W.K. Kegel, H.N.W. Lekkerkerker, R.P.A. Dullens, Soft Matter **5**, 2448 (2009)
109. A. Engelbrecht, H.J. Schöpe, Cryst. Growth Design **10**, 2258 (2010)
110. S. Martin, G. Bryant, W. van Megen, Phys. Rev. E **71**, 021404 (2005)
111. P.N. Pusey, *Liquids, Freezing and Glass Transition*, edited by J.P. Hansen, D. Levesque, J. Zinn-Justin (Elsevier Science Publishers, 1991), p. 763
112. W. Poon, Science **304**, 830 (2004)
113. P.N. Pusey, Science **309**, 1198 (2005)
114. J.C. Crocker, D.G. Grier, J. Colloid Interface Sci. **179**, 298 (1996)
115. M.C. Jenkins, S.U. Egelhaaf, Adv. Colloid Interface Sci. **136**, 65 (2008)
116. R.P.A. Dullens, D.G.A.L. Aarts, W.K. Kegel, H.N.W. Lekkerkerker, Mol. Phys. **103**, 3195 (2005)
117. R.P.A. Dullens, D.G.A.L. Aarts, W.K. Kegel, Proc. Natl. Acad. Sci. (US) **103**, 529 (2006)
118. P.R. ten Wolde, M.J. Ruiz-Montero, D. Frenkel, Faraday Disc. **104**, 93 (1996)
119. P.J. Steinhardt, D.R. Nelson, M. Ronchetti, Phys. Rev. B **28**, 784 (1983)
120. A. Yethiraj, A. van Blaaderen, Nature **421**, 513 (2003)
121. C.P. Royall, W.C.K. Poon, E.R. Weeks, Soft Matter **9**, 17 (2013)
122. W.C.K. Poon, E.R. Weeks, C.P. Royall, Soft Matter **8**, 21 (2012)
123. M. Stieger, J.S. Pedersen, P. Lindner, W. Richtering, J. Chem. Phys. **120**, 6197 (2004)
124. M. Stieger, J.S. Pedersen, P. Lindner, W. Richtering, Langmuir **20**, 7283 (2004)
125. S. Nayak, L.A. Lyon, Angew. Chem. Int. Ed. **44**, 7686 (2005)

126. D. Gottwald, C.N. Likos, G. Kahl, H. Löwen, Phys. Rev. Lett. **92**, 068301 (2004)
127. A.N.S. John, V. Breedveld, L.A. Lyon, J. Phys. Chem. B **111**, 7796 (2007)
128. P.S. Mohanty, W. Richtering, J. Phys. Chem. B **112**, 14692 (2008)
129. J. Riest, P. Mohanty, P. Schurtenberger, C.N. Likos, Z. Phys. Chem. **226**, 711 (2012)
130. M. Muluneh, J. Sprakel, H.M. Wyss, J. Mattsson, D.A. Weitz, J. Phys.: Condens. Matter **23**, 505101 (2011)
131. D. Paloli, P.S. Mohanty, J.J. Crassous, E. Zaccarelli, P. Schurtenberger, Soft Matter **9**, 3000 (2013)
132. B. Sierra-Martin, A. Fernandez-Nieves, Soft Matter **8**, 4141 (2012)
133. H. Senff, W. Richtering, J. Chem. Phys. **111**, 1705 (1999)
134. C.B. Müller, W. Richtering, Coll. Polym. Sci. **286**, 1215 (2008)
135. S. Hoefl, L. Zitzler, T. Hellweg, S. Herminghaus, F. Mugele, Polymer **48**, 245 (2007)
136. M. Dijkstra, R. van Roij, J. Phys.: Condens. Matter **17**, S3507 (2005)
137. B.B. Laird, R.L. Davidchack, J. Phys. Chem. C **111**, 15952 (2007)
138. R. Benjamin, J. Horbach, J. Chem. Phys. **137**, 044707 (2012)
139. R. Ohnesorge, H. Löwen, H. Wagner, Phys. Rev. E **50**, 4801 (1994)
140. J. Hernández-Guzmán, E.R. Weeks, Proc. Natl. Acad. Sci. (US) **106**, 15198 (2009)
141. R.L. Davidchack, B.B. Laird, J. Chem. Phys. **108**, 9452 (1998)
142. M. Oettel, S. Dorosz, M. Berghoff, B. Nestler, T. Schilling, Phys. Rev. E **86**, 021404 (2012)
143. K. Yoshizawa, T. Okuzono, T. Koga, T. Taniji, J. Yamanaka, Langmuir **27**, 13420 (2011)
144. S.M. Ilett, A. Orrock, W.C.K. Poon, P.N. Pusey, Phys. Rev. E **51**, 1344 (1995)
145. A. Cacciuto, D. Frenkel, J. Phys. Chem. B **109**, 6587 (2005)
146. M. Pühse, M. Keerl, C. Scherzinger, W. Richtering, R. Winter, Polymer **51**, 3653 (2010)
147. S. Grobelny, C. Hofmann, M. Erlkamp, F.A. Plamper, W. Richtering, R. Winter, Soft Matter **9**, 5862 (2013)